

Drag prediction and decomposition of a real aircraft based on middle-field and far-field methods

Yeming Deng*, Yufei Zhang*, Haixin Chen *

* School of Aerospace Engineering,

Tsinghua University, Beijing, 100084, China

Abstract

Drag coefficient is a very important aerodynamic performance parameter of an aircraft. The common used method to compute drag coefficient is integrating the pressure and the wall shear stress on the aircraft surface, which is called 'Near-Field Method'. Based on the momentum conservation law, drag can be calculated by integration at a far-field surface or a volume surrounding the aircraft. This paper employs a middle-field method and a far-field method to compute the aerodynamic drag. The methods are validated by CRM, and then applied the methods to a real powered aircraft model. The results show that the middle-field method can get a more precise drag coefficient than the near-field method. The present result shows that, the region below wing and near nacelle is the main contributor of shock wave drag. Thrust loss of the inlet and nozzle are also analyzed.

Nomenclature

S_{Body}	=	aircraft surface, towards the aircraft
S_{Far}	=	far-field surface, towards the outside of flow field
V_{all}	=	flow field between S_{Body} and S_{Far}
V_{shock}	=	shock region
V_{viscous}	=	wake/boundary layer region
V_{spurious}	=	$V_{\text{all}} - V_{\text{shock}} \cup V_{\text{profile}}$
$\vec{n} = (n_x, n_y, n_z)$	=	unit normal vector to a surface
C_d	=	drag coefficient
C_l	=	lift coefficient
ρ	=	density
$\vec{V} = (u, v, w)$	=	velocity vector
V_∞	=	freestream velocity
Δu_{irrev}	=	longitudinal velocity deficit, irreversible part
Ma	=	freestream Mach number
Re	=	freestream Reynolds number
p	=	pressure
D	=	drag force

1. Introduction

Lift and drag coefficients are the most important aerodynamic performance parameters of aircrafts. Many works are spent on improving the accuracy of lift and drag prediction. The traditional method of predicting the coefficients by CFD is integrating the pressure and the wall shear stress on the aircraft's surface, which is called 'Near-Field Method'. The drag coefficient computed by this method is affected by numerical error and diffusion due to the computational mesh and CFD program. Based on the momentum conservation law, two different drag prediction methods can be derived, called 'Middle-Field Method' and 'Far-Field Method'. The former one is based on volume

integration of the space between the aircraft surface and the far field boundary. The latter one is a surface integration of the far field boundary. The near-field, middle-field or far-field methods can divide total drag into different kinds of drags, which is referred to drag decomposition. Paparone and Tognaccini^[1] analyzed the integrands of the middle-field method and the far-field method and expressed the total drag as the sum of wave drag, viscous drag, vortex drag and spurious drag. The far-field method can also decompose total drag into entropy drag (wave drag, viscous drag, spurious drag) and vortex drag.

The near-field method can divide total drag into pressure drag and skin friction drag, which is commonly used. While the far-field method can decompose total drag into entropy drag and vortex drag. Entropy drag is related to irreversible phenomenon, including shock waves and boundary layers. Vortex drag, also called induce drag, is due to reversible phenomenon such as vortex. Middle-field method is derived from far-field method by applying the Gauss's theorem. This method can furtherly decompose entropy drag into wave drag caused by shock wave and profile drag caused by boundary layer by selecting the region of integration. Besides, another drag component, called spurious drag, which is connected with entropy variation due to unphysical phenomenon, can also be separated out by middle-field method.

In this study, the far-field method and middle-field method are applied to a wing-body model as validation. Then a full aircraft configuration with powered-on nacelle is computed by near-field, middle-field and far-field methods. Results of these methods are analyzed.

2. Drag Prediction Methods

In this chapter, three drag prediction methods is concisely introduced, following the strategy of region selection. A Cartesian system is used in the paper with x axis aligned to the freestream velocity vector.

2.1 Near-Field Method

Traditionally, the drag of aircrafts is computed with the pressure and friction on aircraft's surface:

$$D_{\text{near}} = \iint_{S_{\text{body}}} (pn_x - \vec{\tau}_x \cdot \vec{n} + \rho u(\vec{V} \cdot \vec{n}))dS \quad (1)$$

The first and second terms on the right side are pressure drag and friction drag, the positive direction of S_{body} points to the inside of aircrafts. This equation is referred as near-field method.

2.2 Far-field Method

With the momentum balance in x axis, equation(1) can be transferred into a integration at a closed far-field surface:

$$D_{\text{far}} = \iint_{S_{\text{far}}} (-pn_x + \vec{\tau}_x \cdot \vec{n} - \rho u(\vec{V} \cdot \vec{n}))dS \quad (2)$$

The positive direction of S_{far} points to the outside of flow field. If the far-field surface S_{far} is sufficiently far from the aircraft, $\vec{\tau}_x$ can be neglected. Destarac^[2] introduced the irreversible part of axial velocity defect as follows:

$$\Delta u_{\text{irrev}} = u_{\infty} (1 + 2\Delta H / q_{\infty}^2 - 2[\exp((\Delta s / R)(\gamma - 1 / \gamma)) - 1] / (\gamma - 1)M_{\infty}^2)^{1/2} - u_{\infty} \quad (3)$$

In equation (3), Δs and ΔH are entropy and total enthalpy relative to freestream value. R and γ are gas constant and specific heat ratio, separately. In far field area, if no vortex (reversible phenomenon) is generated by the aircraft, Δp should be zero and the velocity direction should be the same as the freestream direction. Then irreversible and reversible components of drag are:

$$D_{\text{far,irrev}} = \iint_{S_{\text{far}}} -\Delta u_{\text{irrev}} \rho (\vec{V} \cdot \vec{n}) dS \quad (4)$$

$$D_{\text{far,rev}} = \iint_{S_{\text{far}}} (-pn_x - \rho(u - \Delta u_{\text{irrev}})(\vec{V} \cdot \vec{n})) dS \quad (5)$$

Define \vec{F}_{irrev} and \vec{F}_{rev} :

$$\vec{F}_{\text{irrev}} = -\Delta u_{\text{irrev}} \rho \vec{V}, \quad \vec{F}_{\text{rev}} = -p\vec{i} - \rho(u - \Delta u_{\text{irrev}}) \vec{V} \quad (6)$$

Then

$$D_{\text{far,rev}} = \iint_{S_{\text{far}}} \vec{F}_{\text{rev}} \cdot \vec{n} dS \quad (7)$$

$$D_{\text{far,irrev}} = \iint_{S_{\text{far}}} \vec{F}_{\text{irrev}} \cdot \vec{n} dS \quad (8)$$

Equation (7) and (8) is referred as far-field method of unpowered aircraft. The irreversible part is due to shock waves, boundary layers. It is also called entropy drag. The reversible part corresponds to vortex, so this part is also named as induced drag.

2.3 Middle-field Method

Apply the Gauss's theorem to irreversible part of far-field method, notice \vec{V} is zero at the surface of unpowered aircraft, then:

$$D_{\text{middle,irrev}} = \iiint_{V_{\text{all}}} \vec{\nabla} \cdot \vec{F}_{\text{irrev}} dV \quad (9)$$

Equation(9) is entropy drag of unpowered aircraft by the middle-field method. For a powered aircraft, \vec{V} is not zero at the inlet and outlet boundary surfaces, so equation (9) need to change. Define S_{in} and S_{out} as inlet and outlet boundary of a powered aircraft separately, then the remaining surface of the aircraft is $S_{\text{skin}} = S_{\text{body}} - S_{\text{in}} - S_{\text{out}}$. Then the drag balance becomes

$$\begin{aligned} D_{\text{far}} &= \iint_{S_{\text{far}}} \vec{F}_{\text{rev}} \cdot \vec{n} dS + \iint_{S_{\text{far}}} \vec{F}_{\text{irrev}} \cdot \vec{n} dS \\ &= \iint_{S_{\text{far}}} \vec{F}_{\text{rev}} \cdot \vec{n} dS + \iint_{S_{\text{far}}} \vec{F}_{\text{irrev}} \cdot \vec{n} dS + \iint_{S_{\text{body}}} \vec{F}_{\text{irrev}} \cdot \vec{n} dS - \iint_{S_{\text{in}} + S_{\text{out}}} \vec{F}_{\text{irrev}} \cdot \vec{n} dS \\ &= \iint_{S_{\text{far}}} \vec{F}_{\text{rev}} \cdot \vec{n} dS + \iiint_{V_{\text{all}}} \vec{\nabla} \cdot \vec{F}_{\text{irrev}} dV - \iint_{S_{\text{in}} + S_{\text{out}}} \vec{F}_{\text{irrev}} \cdot \vec{n} dS \end{aligned} \quad (10)$$

2.3.1 Region Selection Strategy

As discussed by Paparone et al.^[1], the integrand of equation (9) associates to the entropy production rate per unit volume, so entropy drag components caused by different physical phenomenon can be separated by specifying different integral regions.

To select the region producing shock wave drag, the sensor introduced by Paparone is widely used:

$$f_{\text{shock}} = \frac{\vec{V} \cdot \nabla p}{a |\nabla p|} \quad (11)$$

In equation (11), a is local sound speed. The sensor f_{shock} represents the local Mach number component in the direction of local pressure gradient. In numerical simulations, a shock wave is not a discontinuity of physical variables, but a change of variables in several grid cells. Therefore, the value is above 1 at the close neighborhood of a shock wave and is negative in expansion zones. Besides, if the freestream is subsonic and the speed is not too close to the speed of sound, f_{shock} will only be greater than one at shock waves. For there is numerical oscillation in CFD, the upwind and downstream of a shock wave should also be selected as shock wave drag region, and an extension of shock region is needed.

The component of drag due to shock wave is expressed as:

$$D_{\text{middle,shock}} = \iiint_{V_{\text{shock}}} \nabla \cdot \vec{F}_{\text{irrev}} dv \quad (12)$$

V_{shock} is the region selected as shock wave drag region. Apart from shock wave, the other physical process producing irreversible drag in unpowered system are boundary layer and shear layer in wake region, this part of drag is called profile drag or viscous drag. Paparone gives a sensor based on dynamic viscosity and eddy viscosity. Lanzetta^[3] introduced new selection strategies of profile drag region, analyzed and compared the strategies to find a sensor based on dissipation of turbulence kinetic energy to be the best one, which is defined as:

$$f_{\text{viscous}}^* = \log_{10}(S_{\text{ble}} / Ma_{\infty}^3) \quad (13)$$

Where

$$S_{\text{ble}} = \rho \varepsilon = \mu \left[\overline{\left(\frac{\partial u'}{\partial x} \right)^2} + \overline{\left(\frac{\partial v'}{\partial x} \right)^2} + \overline{\left(\frac{\partial w'}{\partial x} \right)^2} + \overline{\left(\frac{\partial u'}{\partial y} \right)^2} + \overline{\left(\frac{\partial v'}{\partial y} \right)^2} + \overline{\left(\frac{\partial w'}{\partial y} \right)^2} + \overline{\left(\frac{\partial u'}{\partial z} \right)^2} + \overline{\left(\frac{\partial v'}{\partial z} \right)^2} + \overline{\left(\frac{\partial w'}{\partial z} \right)^2} \right] \quad (14)$$

In boundary layer and shear layer, the value of f_{viscous}^* is approximately above -9. Due to the same reason described about shock drag region selection, an extension of area is also needed for the selection of profile drag region. For the region both at a shock wave and in a boundary layer, the drag is considered to be profile drag region.

The expression of profile drag is

$$D_{\text{middle,profile}} = \iiint_{V_{\text{profile}}} \nabla \cdot \vec{F}_{\text{irrev}} dv \quad (15)$$

in which V_{profile} is the region of profile drag. If a cell can be detected as both shock drag and profile drag, then this cell is marked as profile drag.

After selecting the shock wave and profile drag zones, the remaining area don't contain irreversible process and should not produce irreversible drag. But due to artificial viscosity, numerical error and grid feature, $\nabla \cdot \vec{F}_{\text{irrev}}$ in the remaining area maybe not zero, so the irreversible drag produced there is called spurious drag. The expression of spurious drag is

$$D_{\text{middle,spurious}} = \iiint_{V_{\text{spurious}}} \nabla \cdot \vec{F}_{\text{irrev}} dv \quad (16)$$

The domain of integration is $V_{\text{spurious}} = V_{\text{all}} - V_{\text{shock}} \cup V_{\text{viscous}}$

Now entropy drag can be separated as follows:

$$\begin{aligned} D_{\text{middle,irrev}} &= \iiint_{V_{\text{shock}}} \vec{\nabla} \cdot \vec{F}_{\text{irrev}} dV + \iiint_{V_{\text{viscous}}} \vec{\nabla} \cdot \vec{F}_{\text{irrev}} dV + \iiint_{V_{\text{spurious}}} \vec{\nabla} \cdot \vec{F}_{\text{irrev}} dV \\ &= D_{\text{wave}} + D_{\text{viscous}} + D_{\text{spurious}} \end{aligned} \quad (17)$$

The regions are illustrated in Figure 1.

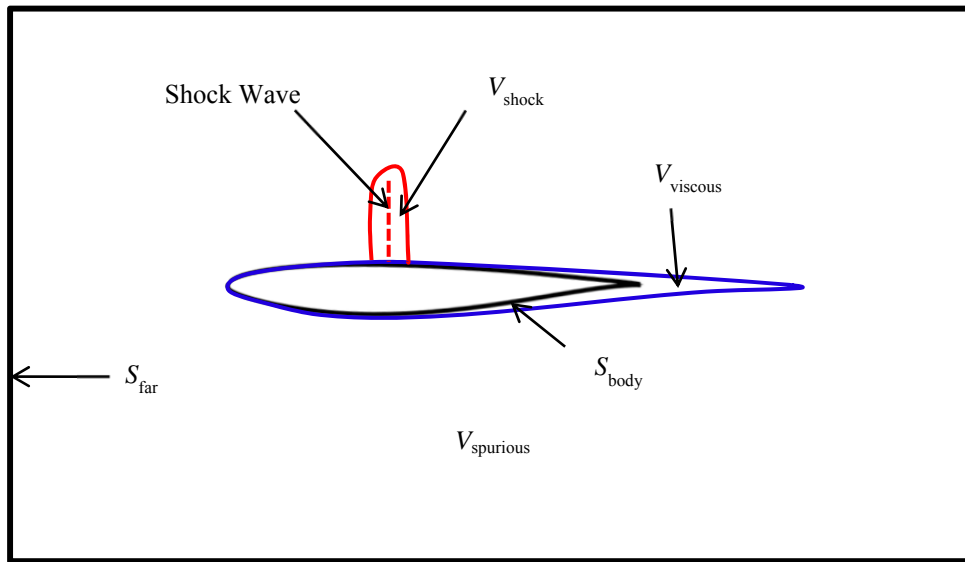


Figure 1: Region selection

3 Flow Solver & CFD Test Cases

3.1 Flow-field Simulation Software, NSAWET

NSAWET is an in-house flow solver for three-dimensional unsteady compressible Euler or Navier-Stokes equations based on finite volume method and multi-block structured grid. The program has been successfully used to simulate and analyze various aerodynamics cases. All the flow field data in this study are obtained by using NSAWET to solve the steady Reynolds Averaged Navier-Stokes (RANS) equations. For spatial discretization, the third-order Monotone Upstream centered Scheme for Conservation Laws (MUSCL) scheme^[4] (with Venkatakrishnan limiter^[5]) and Roe's FDS flux^[6] (with Radespiel-Swanson entropy fix^[7]) are used. The viscous term is discretized by second-order central differencing. The implicit Lower-Upper Symmetric Gauss-Seidel (LU-SGS) method^[8] is chosen for efficient time iteration. For RANS simulations, the Menter's $k-\omega$ -SST model^[9] is used.

3.2 CFD Test Cases

Firstly, the NASA's Common Research Model (CRM) is used to verify the middle-field and far-field method based on NSAWET. Then the methods are used to analyze a real powered aircraft.

The surface mesh of CRM is shown in Figure 2. The free stream Mach number is 0.85, Reynolds number based on mean aerodynamic chord is 5×10^6 . The angles of sideslip is 0, and lift coefficient of CRM is set to be 0.5 and the angle of attack is alterable.

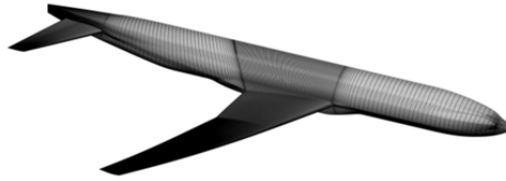


Figure 2: Mesh of CRM

Surface mesh of a real powered aircraft is shown in Figure 4, and the angles of attack and sideslip are 0.

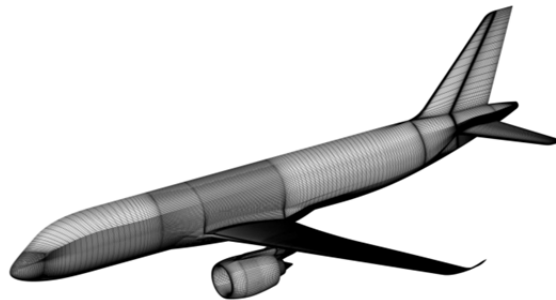


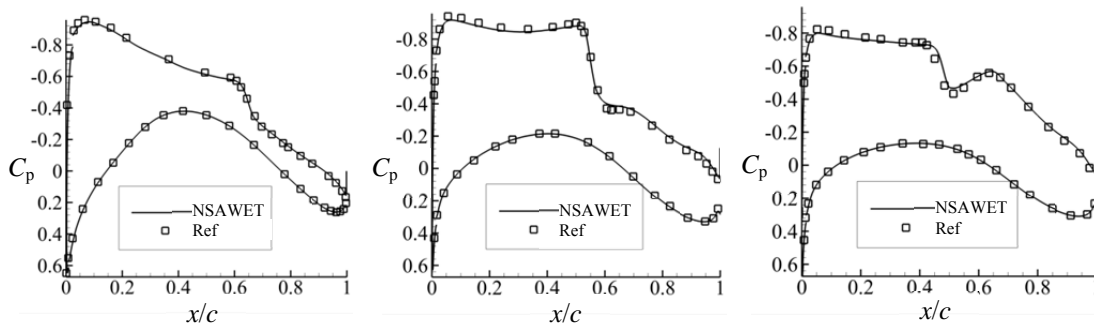
Figure 3: Mesh of powered aircraft

The free stream Mach number is 0.785, Reynolds number based on mean aerodynamic chord is 2.4×10^7 . The inlet of engine is set with static pressure, and the outlet is set with total temperature and total pressure. Since the angles of sideslip of both cases are zero, half-model with symmetric boundary condition is used to save computing resource. The y^+ of first layer mesh in both cases are below 1.

4 Result & Analysis

4.1 Case 1: CRM

Pressure distribution of medium mesh is shown in Figure 4. At different semi-span position fraction at wing, the pressure results are compared with result from reference 10.



(a) semi-span position fraction 0.201 (b) semi-span position fraction 0.502 (c) semi-span position fraction 0.846

Figure 4: Pressure distribution

After analyzing flow field around aircraft with equation (12), the contour of entropy drag source at a certain position

of wing is illustrated in Figure 5.

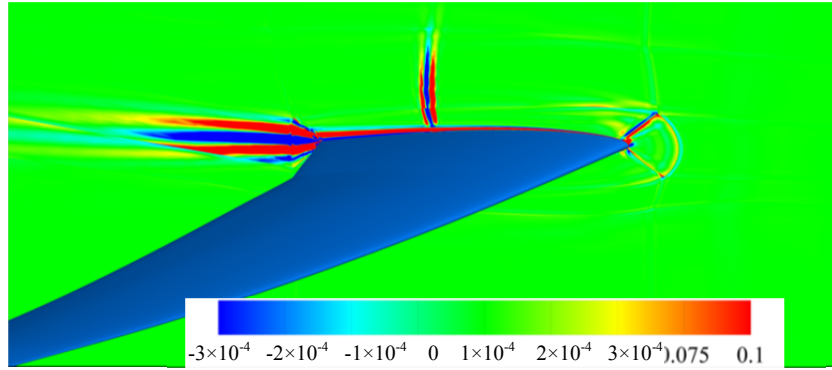


Figure 5: $\nabla \cdot \vec{F}_{\text{irrev}}$ contour of CRM

With the drag decomposition strategy, we can decompose entropy drag into wave drag, viscous drag and spurious drag. Comparing Figure 5 with the distribution of sensors of shock wave and profile drag in Figure 6, the drag source distribution matches the shock drag region and viscous drag region.

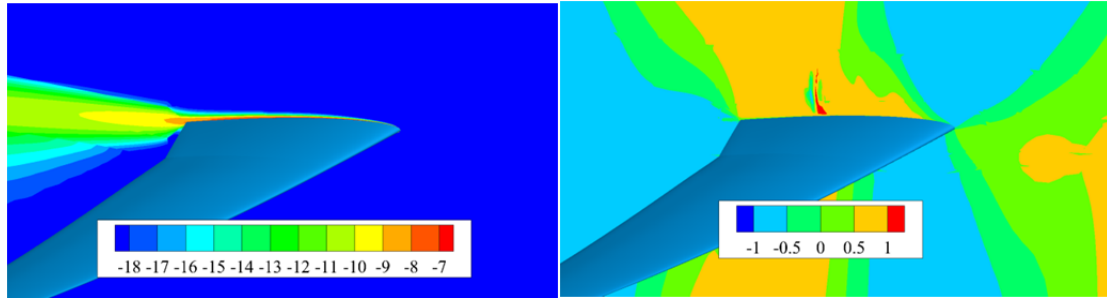


Figure 6: f_{viscous}^* contour (left) and f_{shock} contour (right) of CRM

Notice that in flow field result of CFD, shock wave is not a discontinuity between two cells, but a phenomenon distributed in some grid cells along the flow direction. Besides, format error may cause the region of entropy drag source to expand. So, the result of region selection should be a little wider than the region selected by $f_{\text{shock}} > 1$ and $f_{\text{viscous}}^* > -9$.

After selecting the regions of different source of entropy drags, viscous drag and shock drag distribution at a certain span position is shown in Figure 7.

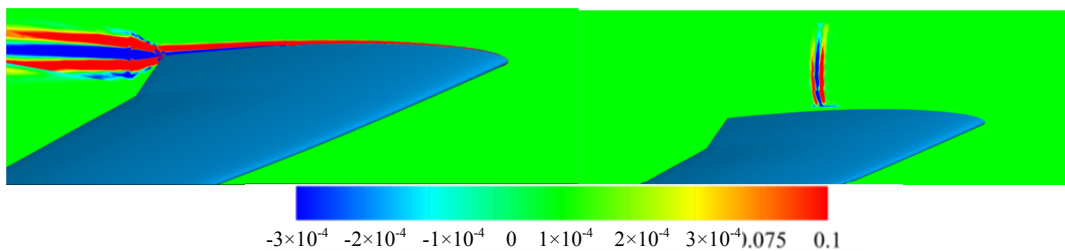


Figure 7: Viscous drag (left) and Shock drag (right) contours at a certain span position

The envelope surfaces of shock drag and viscous drag is shown in Figure8

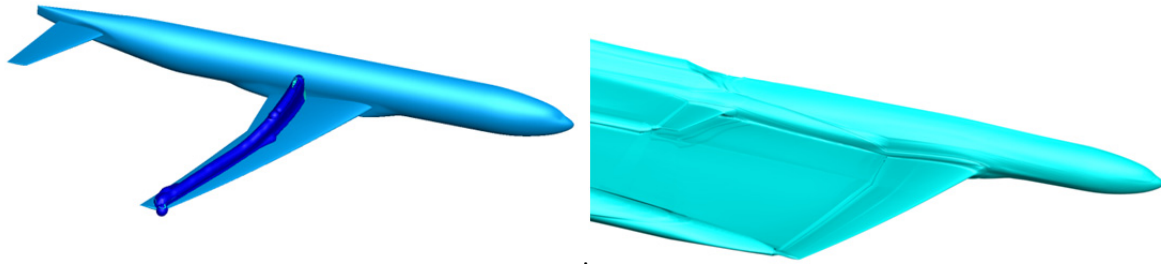


Figure 8: Envelope surfaces viscous drag (left) and shock drag (right)

Region apart from the two kinds above contributes to spurious drag. Main location of spurious drag is shown in Figure 9. As shown in the figure, spurious drag appears mainly at the leading edge of main wing, horizontal wing and the nose.

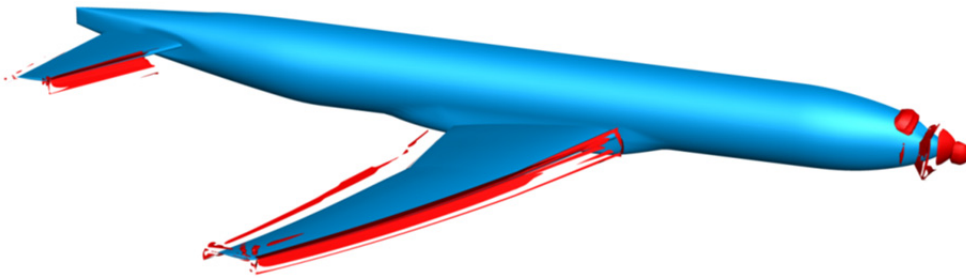


Figure 9: Main location of spurious drag

Contours of spurious drag around nose and leading edge of main wing is shown in Figure 10. It's obvious that large growing rate of mesh generate spurious drag.

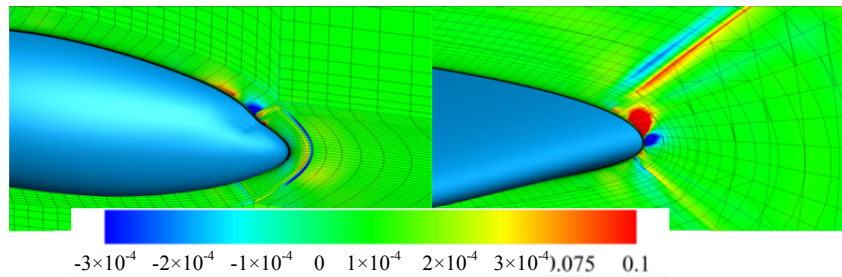


Figure 10: Spurious drag contour

As discussed above, shock wave drag, viscous drag and spurious drag are entropy drag, i.e. irreversible drag. The reversible drag caused by induced vortex can be calculated by equation (7). In theory, the shear flow within the vortex will weaken the induced vortex gradually and the kinetic energy of the vortex is transformed into the internal energy of the air. This process will gradually convert reversible drag of the induced vortex into irreversible drag. But in numerical simulation, due to the artificial viscosity and numerical error, the induced vortex becomes weaker along the wake faster than reality, thus the process of reversible drag becoming irreversible drag is faster than reality. Although the induced resistance will gradually be transformed into entropy drag, but the sum remains unchanged. So induced drag should be the sum of induce drag from equation (7) and entropy drag from shear flow due to induced vortex. In this paper, integration surface of induce drag is based on CFD mesh and this part of reversible drag is calculated with far-field method. Entropy drag part of induced drag is a volume integration of $\nabla \cdot \vec{F}_{\text{irrev}}$ from middle-field method in the area after the aircraft in the direction of free stream. Results about induced drag are shown in Figure 11.

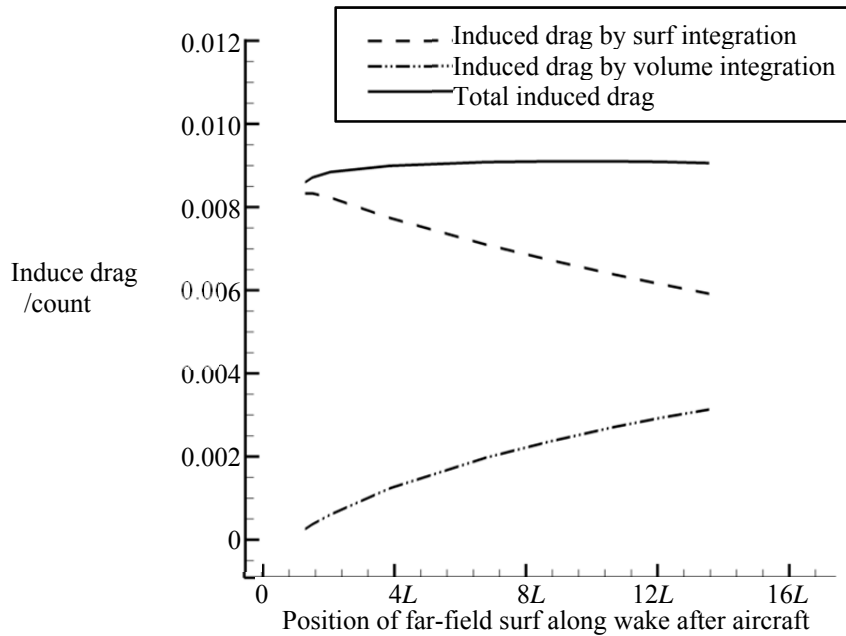


Figure 11: Different part of induced drag along wake

The C_d result is shown in table 1. With far-field method, we successfully decompose total drag into total drag of aircraft into shock drag, viscous drag, induced drag and spurious drag. The results of both near-field and far-field are all close to the result from reference 10.

Table 1: Drag efficient of CRM

Type of drag	value/count
Total drag by near-field method	267.3
Shock drag	5.0
Viscous drag	180.9
Induced drag	87.0
Total drag by far-field method	273.4
Average of total drag in Ref	270

4.2 Case 2: Powered aircraft

The procedure of drag decomposition of case 2 is similar to case 1. The envelope surface of shock drag and viscous drag are shown in Figure 12. Since the angle of attack is 0 and lift coefficient is not large, the shock wave region above the wing is small.

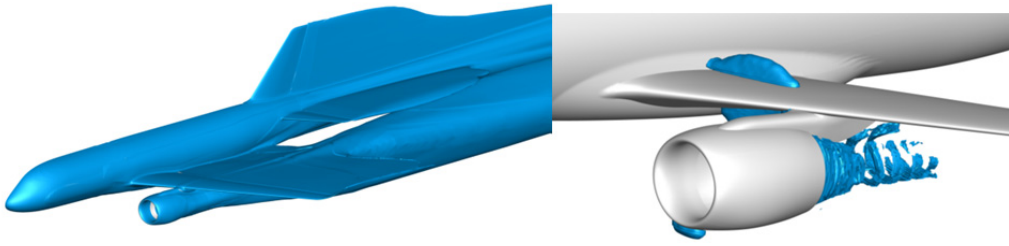


Figure 12: Viscous drag region (left) and shock drag region (right) of powered aircraft

Since entropy drag of middle-field method is calculated by volume integration, shock drag of different region can be separated by the integration position. The shock drag at different position is given in Table 1

Table 1: Shock drag at different position

Position	Shock drag/count
Above wing	0.1
Below wing, out of jet	3.7
In jet	1.7
Near nacelle lip	0.2
Total shock drag	5.7

Because the angle of attack is 0, shock wave above the wing is weak. But the location between wing and nacelle generate about 3.7 count of shock drag. It is caused by the contraction-expansion channel formed by the wing and nacelle. The main position of spurious drag is illustrated in Figure 13

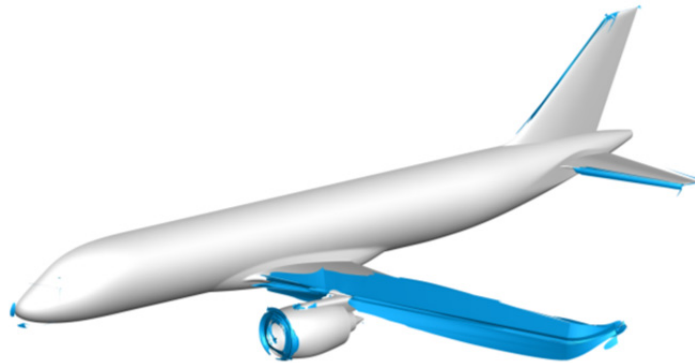


Figure 13: Main spurious drag region

Similar to test case 1, spurious drag of test case 2 is mainly generated around leading edges of wings and nacelle. Since test case 2 is a powered aircraft, thrust-drag bookkeeping is important. In this paper, the entropy drag generated in the inlet and nuzzle is marked as loss of thrust, the location is illustrated with black line in Figure 14.

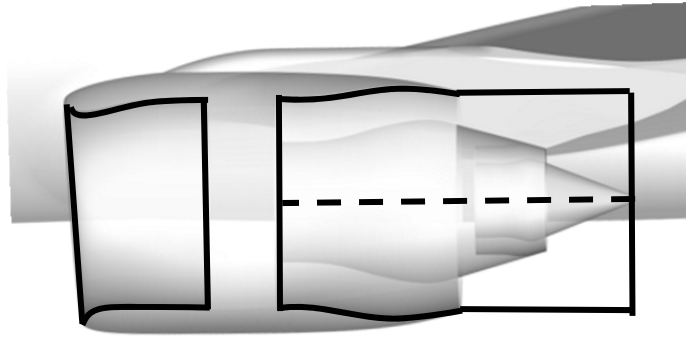


Figure 14: Thrust loss region

The drag and thrust result is given in Table 2

Table 2: Drag and thrust of powered aircraft

Drag or thrust	Value/count
Drag at skin	410
Thrust at inlet and outlet	565
Thrust loss in inlet and nuzzle	25
Thrust-Loss	540
Total force	225(forward)

5 Conclusion

In this paper, middle-field method and far-field methods are applied to CRM and a real aircraft. The middle-field and far-field methods get better drag result compared to near-field method. For powered aircraft, shock drag at different positions is calculated separately by middle-field method. Shock wave generated below the wing near the nacelle is significant. The thrust loss is calculated by middle-field method.

In the future, the middle-field and far-field method can be used to optimize computational mesh and can also be apply to unpowered model of the aircraft analyzed in this paper, in order to compare the shock drag under the wing and analyze the jet's influence on drag distribution.

References

- [1] Paparone L, Tognaccini R. Computational Fluid Dynamics-Based Drag Prediction and Decomposition[J]. *AIAA Journal*, 2003, 41(9):1647-1657..
- [2] Destarac D, Vooren J V D. Drag/thrust analysis of jet-propelled transonic transport aircraft; Definition of physical drag components[J]. *Aerospace Science & Technology*, 2004, 8(6):545-556.
- [3] Lanzetta M, Mele B, Tognaccini R. Advances in Aerodynamic Drag Extraction by Far-Field Methods[J]. *Journal of Aircraft*, 2015, 52(6).
- [4] Van Leer, B., "Towards the Ultimate Conservative Difference Scheme. V. A Second-Order Sequel to Godunov's Method," *Journal of Computational Physics*, 1979, 32: 101-136.
- [5] Venkatakrisnan, V., "Convergence to Steady-State Solutions of the Euler Equations On Unstructured Grids with Limiters," *Journal of Computational Physics*, 1995, 118: 120-130

- [6] Roe, P.L., "Characteristic-Based Schemes for the Euler Equations," *Annual Review of Fluid Mechanics*, 1986, 18: 337-365
- [7] Radespiel, R., and Swanson, R.C., "Progress with Multigrid Schemes for Hypersonic Flow Problems," *Journal of Computational Physics*, 1995, 116: 103-122.
- [8] Yoon, S., and Jameson, A., "Lower-Upper Symmetric-Gauss-Seidel Method for the Euler and Navier-Stokes Equations," *AIAA Journal*, 1988, 26: 1025-1026
- [9] Menter, F.R., "Two-Equation Eddy-Viscosity Turbulence Models for Engineering Applications," *AIAA Journal*, 1994, 32: 1598-1605.
- [10] Vassberg J C, Tinoco E N, Mani M, et al. Summary of the fourth AIAA computational fluid dynamics drag prediction workshop [J]. *Journal of Aircraft*, 2014, 51(4): 1070-1089.